Journal of Catalysis **192,** 11–17 (2000)
doi:10.1006/jcat.2000.2813, available online at http://www.idealibrary.com on IDEAL®

Simulation of MEIS Spectra for Quantitative Understanding of Average Size, Composition, and Size Distribution of Pt–Rh Alloy Nanoparticles

I. Konomi, S. Hyodo, and T. Motohiro

Toyota Central Research and Development Laboratories, Inc., Nagakute, Aichi 480-1192, Japan
E-mail: konomi@mosk.tytlabs.co.jp

Received July 13, 1999; revised January 3, 2000; accepted January 6, 2000

We have newly developed a medium-energy ion scattering (MEIS) simulation program for the analysis of alloy nanoparticles. The program was applied to the composition and average particle size analysis of Pt–Rh/α-Al_2O_3 treated in oxidative and reductive atmospheres. It was found that the Pt concentration near the surface decreased after oxidative treatment at 800°C and returned to its original value after reductive treatment at the same temperature. It was shown that Pt particle average sizes less than 10 nm can be evaluated quantitatively. Also, this technique gives some insight into particle size distribution in the initial stage of particle sintering, which has been quite out of the reach of conventional analytical tools.

Key Words: **medium-energy ion scattering; spectrum simulation; metal particle; Pt; Pt–Rh; catalysis; surface composition; sintering; particle size distribution.**

1. INTRODUCTION

In automobile emissions control, it has been of great importance to develop catalysts which have good thermal stability and high NO_x conversion. To achieve this goal, it is crucially important to understand the behavior of metal particles and supports in engine exhaust gas.

A catalyst has a structure in which metal particles such as Pt and Rh are supported on a support material such as Al_2O_3. The metal particles are exposed to an oxidative or a reductive environment repeatedly, and surface segregation of constituent atoms and growth of metal particles can take place.

Catalytic activity is related to two factors; one is surface composition and the other is surface area. Surface segregation changes the surface composition, leading to changes of the chemisorption property, affecting the catalytic activity directly. Growth of metal particles causes the reduction of the surface area, which also changes catalytic activity (1). Therefore, it is of great importance to estimate both the surface segregation and the particle growth quantitatively.

Conventionally, X-ray diffraction (XRD) and gas adsorption (2–4) have been utilized in the evaluation of the size of metal particles on highly porous supports. From the full width at half maximum of a peak in XRD spectrum, average particle size can be obtained according to Scherrer's equation (5). In the gas adsorption method, particle size is estimated from the total number of metal atoms and the number of adsorbed atoms. Atomic force microscopy (AFM) was used recently to observe metal particle growth on flat surfaces (6). AFM can determine not only the average particle size but also the distribution of particle sizes. For sizes below 10 nm, however, these methods are often unsuccessful in evaluating the particle diameter. In this size range, transmission electron microscopy (TEM) is widely used with considerable elaboration in sample preparation.

Medium-energy ion scattering (MEIS) is a method of surface analysis which can determine elemental composition and crystalline lattice disorder as a function of depth (7, 8). In MEIS measurement, an ion beam such as H^+ or He^+ is impinged onto a surface and is scattered after colliding with sample atoms. The energy of scattered ions is measured with an electrostatic analyzer and is related to the depth at which the corresponding ions were scattered. Typical analyzing depth is about 100 nm, and depth resolution (which is determined by the high-energy edge of a spectrum for an element) is about 0.5 nm at the surface.

Taking advantage of its excellent depth resolution, we can utilize MEIS for the estimation of surface composition and the size of metal nanoparticles. For this purpose, we have developed a MEIS simulation program for metal particles for the first time. After describing the physical basis for the simulation and the simulation procedure, we propose some examples of the analysis of the surface segregation of Pt–Rh alloy particles and particle growth of Pt metal particles on an α-Al_2O_3 substrate and estimate the simulation's applicability to the determination of surface composition and metal particle sizes.

2. SIMULATION METHOD

When incident He ions are scattered by the atoms of the *i*th element in a small volume *dv* in a metal (or alloy)

0021-9517/00 $35.00

particle, the number of detected ions $H_i(E_{\text{out}})\,dE$ is described as

$$\begin{aligned} H_i(E_{\text{out}})\,dE &= x_i\, Q\Omega\sigma_i(E_{\text{in}},\theta)N\,dv, \\ E_{\text{in}} &= E_0 - E_{\text{lossin}}(x,y,z), \\ E_{\text{out}} &= E_{\text{in}} - E_{\text{lossout}}(x,y,z), \end{aligned} \qquad [1]$$

where x_i is the composition of the ith element, E_0 is incident energy, E_{in} is ion energy just before scattering, $E_{\text{lossin}}/E_{\text{lossout}}$ is energy loss before/after the scattering of an atom at position (x, y, z) in the metal particle, Q is the dose of He ions, Ω is the solid angle subtended by a detector, $\sigma_i(E_{\text{in}}, \theta)$ is the differential scattering cross section for an atom of the ith element, and N is the atomic density of the metal particle. By integrating the formula [1] over an entire metal particle and summing up for all elements in the metal particle, the MEIS spectrum $H(E)$ for one metal (or alloy) particle is obtained.

To carry out the calculation of formula [1] in the conventional simulation method for thin film analysis, the sample was divided into many slabs in the direction of the surface normal, the spectrum from each slab was calculated, and finally the spectra from all the slabs were synthesized. However, in the case of the metal particle samples, the method mentioned above cannot be used, for two reasons. One reason is that metal particles do not necessarily have the same size but do have a kind of size distribution. The other is that even if metal particles are the same size, the metal particle density per unit area of the support is not necessarily uniform. Therefore, in the present study, we utilized the Monte Carlo method for the calculation of formula [1].

Figure 1 presents the model for ion scattering from a metal particle. For simplicity, the particle is assumed to be a hemisphere in the simulation.

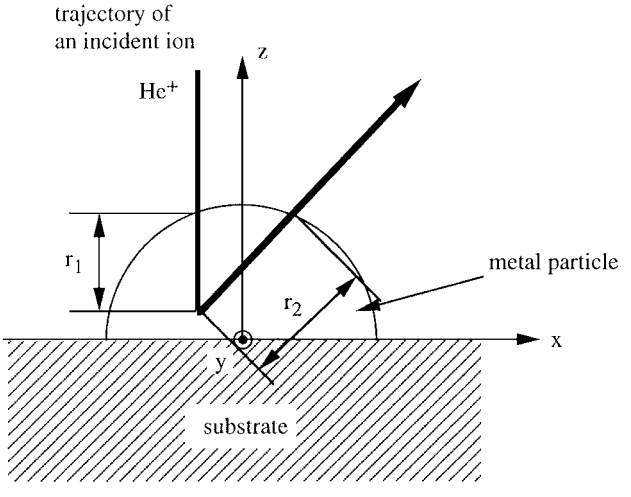

FIG. 1. Hemisphere model of a metal particle for the MEIS simulation.

The simulation procedure is briefly summarized as follows:

(1) The position in a metal particle where scattering occurs is given by (x, y, z) in a hemisphere (radius $= r$). x, y, and z are generated by random numbers. Since scattering probability is proportional to elemental composition and scattering cross section, the number of scattered ions is weighted by the composition and scattering cross section $x_i\,\sigma_i\,(E_{\text{in}}, \theta)$.

(2) The distance between the incident site and the scattering site is calculated, and the E_{lossin} before scattering is calculated from the stopping power (9).

(3) Energy just after scattering is calculated based on kinematical factors according to the physics of atomic scattering.

(4) The E_{lossout} in the outgoing path is calculated from stopping power and E_{out} is determined.

(5) Energy loss has a distribution centered around the average energy E_{out} because of energy straggling (9). Therefore, straggling in the incoming or outgoing path must be calculated. Energy dispersion resulting from the detection system resolution is also taken into account. Energy distribution is assumed to be Gaussian $f(E - E_{\text{out}}, \Gamma)$ with the full width at half maximum (FWHM) Γ.

(6) In general, some of the scattered ions are neutralized on a sample surface. Since we employ an electrostatic energy analyzer which can measure the energy of charged particles only, we must introduce a correction factor $F^+(E)$ (1-neutralization probability) in the simulation procedure to compare the simulated spectrum with the experimental one.

After the calculation mentioned above, the yield of ions detected after scattering from the atoms of the ith element can be described as

$$H_i(E) = x_i\sigma_i(E_{\text{in}},\theta)\; f(E - E_{\text{out}}, \Gamma)F^+(E). \qquad [2]$$

(7) The calculation is performed for a large number of incidence of ions. Each energy distribution is convoluted to generate the MEIS spectrum $H_i\,(E)$ for the ith element. Summing up the $H_i\,(E)$ for all the elements generates the MEIS spectrum $H_r\,(E)$, which corresponds to the spectrum for the metal particle whose radius is r.

Real samples consist of many particles of various sizes having a particle size distribution (6). To take this fact into consideration, we divide particle sizes into several groups and calculate the spectrum for each group. In the last step, we synthesize each spectrum. In this process, the number of metal particles for each size was weighted to the corresponding spectrum height; that is, the synthesized spectrum is described as

$$H_s(E) = \sum_i n_i H_{r_i}(E), \qquad [3]$$

where n_i is the number of the particle whose particle size is r_i, $H_{r_i}(E)$ is the spectrum for a particle whose particle size is r_i, and $H_s(E)$ can be directly compared with a spectrum obtained experimentally.

In this program, the change in the size and the composition of metal particles was calculated, and simulation from the substrate was not taken into consideration. Therefore, this program is supposed to be applied only to a heavy metal/light substrate system. In a light metal/heavy substrate system, the spectrum from the substrate overlaps that from the metal particles, which makes the experimental spectrum difficult to compare with the simulated one.

Now, we describe some of the important physical quantities as follows:

2.1. Scattering Cross Section

When the energy of probing ions is in a high-energy region (more than 500 keV) a Rutherford scattering cross section which is calculated with a Coulomb potential can be used. As the energy of probing ions decreases and the number of electrons of target atoms becomes larger, the screening effect of the electrons on the scattering cross section emerges, and the real scattering cross section begins to deviate from the Rutherford scattering cross section. Therefore, cross sections were calculated by using the Molière potential (10) at each target element and energy. Figure 2 displays the calculated scattering cross sections for Pt and Rh. In the simulation program, $\sigma(E)$ was calculated as a function of energy from the following formula, in which the parameters C_1–C_5 are determined by fitting the real cross section:

$$\sigma(E) \sim \sigma'(E) = C_0 + C_1/E + C_2/E^2 + C_3/E^3 + C_4/E^4 + C_5/E^5. \quad [4]$$

The values of C_1–C_5 for Pt and Rh are shown in Table 1.

2.2. Energy Loss

Ziegler's formula (9) for stopping power was used to calculate the energy loss. In Fig. 1, the probing-ion path before and after collision are shown. The energy of the detected ions is obtained as

$$E_{\text{out}} = K(E_0 - r_1 S(E_0)) - r_2 S(K E_0), \quad [5]$$

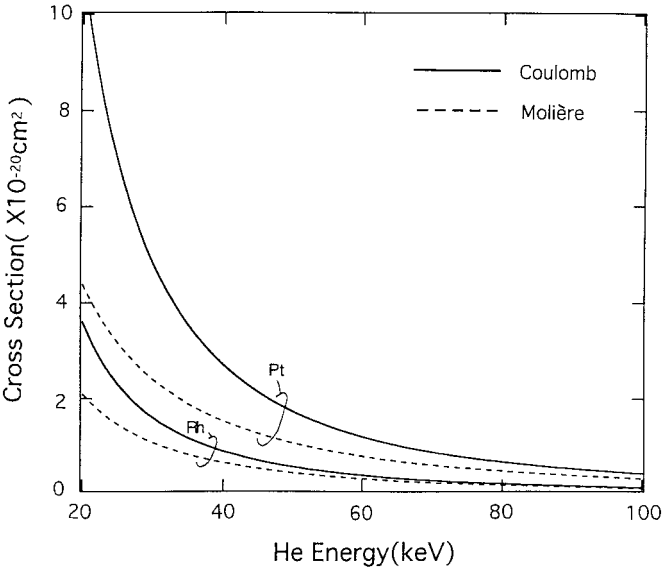

FIG. 2. Differential cross sections for He^+ scattered to 135° from Pt and Rh. The solid and dashed curves are the calculated values using Coulomb and Molière potentials, respectively.

where r_1 is the distance from the incident site to the scattering site, r_2 is the distance between the scattering site and the outgoing site (the dimension of r_1, r_2 is cm^{-2}), and S is the stopping power.

2.3. Energy Straggling

Energy spread due to energy straggling can be calculated with Bohr's formula (11) in a high-energy region. The FWHM Γ_B of Bohr's energy straggling is given as

$$\Gamma_B = 4\pi(8\pi \ln 2) Z_1^2 Z_2 e^4 N\, dt, \quad [6]$$

where e is the electronic charge, Z_1 and Z_2 are the atomic numbers of the incident particle and the target atom, respectively, and N is the atomic density of a metal particle. The length which an incident ion travels is expressed as dt. In the medium-energy region, however, Bohr's formula, which assumes all the target electrons to be free electrons, cannot be used because energy straggling due to inner-shell electrons in the target atoms decreases. Energy straggling, which was calculated using the radial distributions of bound electrons based on the Hartree–Fock–Slater model, was proposed by Chu (12). In the simulation, straggling was

TABLE 1

Constants Used in the Calculation of the Approximated Cross Section Based on Molière Potential

	C_0	C_1	C_2	C_3	C_4	C_5
Rh	−388.815	79302.3	9.250243×10^6	-5.08356×10^7	1.02218×10^8	-4.03559×10^7
Pt	−872.621	208790	2.31466×10^7	-2.62195×10^8	1.68059×10^9	-4.04930×10^9

calculated with Chu's value approximated by the formula (13)

$$\Gamma_s/\Gamma_B = 1.0 - a\exp(-bE)/E, \qquad [7]$$

where a and b are determined for each element.

The energy loss and straggling of samples which consisted of more than two kinds of elements were calculated by Bragg's rule (11).

Using the energy straggling described above, the energy distribution of detected ions is expressed as

$$f(E) = 2\sqrt{\ln 2}/\sqrt{\pi\Gamma(r)}\exp(-4\ln 2(E - E(r))^2/\Gamma(r)^2), \qquad [8]$$

where E is the energy, r is the path length of the ion, and $E(r)$ and $\Gamma(r)$ are the average energy and the FWHM of the energy distribution after passage through a distance r in a metal particle, respectively. The $\Gamma(r)$ is described as

$$\Gamma^2(r) = \Gamma_0^2 + K^2\Gamma_{in}^2 + \Gamma_{out}^2, \qquad [9]$$

where Γ_0 is the FWHM of the energy spread due to the instrumental system resolution and Γ_{in} and Γ_{out} are the FWHM of the energy straggling associated with incoming and outgoing paths, respectively.

2.4. Ion Neutralization

In order to take account of ion neutralization, the simulated yield of scattered ions was multiplied by the correction factor $F^+(E)$ according to the experimental data of Marion and Young (13, 14):

$$F^+(E) = 0.02045(E - 12.3388)^{2/3}. \qquad [10]$$

3. APPLICATION OF THE MEIS SPECTRUM SIMULATION TO METAL PARTICLES

3.1. Compositional Analysis Near the Surface Region

MEIS spectrum of Pt–Rh/α-Al_2O_3. Pt–Rh crystallites were fabricated on an α-Al_2O_3 substrate by electron beam evaporation of Pt and Rh followed by heat treatment at 500°C for 30 min in vacuum. Rutherford backscattering spectroscopy (RBS) analysis of the sample (6) confirmed that Pt–Rh alloy particles (not Pt or Rh single-element particles) are formed by this process. The ratio of the numbers of atoms determined by RBS was Pt : Rh = 0.20 : 0.80.

MEIS measurement was performed using an ion beam of 60 keV He^+ at a scattering angle of 135°. The energy of the scattered ions was analyzed with an electrostatic analyzer, the energy resolution of which was $\Delta E/E = 4 \times 10^{-3}$ (15).

Spectrum simulation was performed assuming the particle radius and composition of a metal particle. Here, the particle radius is given in cm^{-2}. This is because, in MEIS measurement, the quantity which has the dimension of length is given in cm^{-2} (length (cm) × atom density (cm^{-3})), taking into account the atomic density of the metal particle (11). To convert cm^{-2} into cm, the radius described in cm^{-2} must be divided by the atom density of the metal particle.

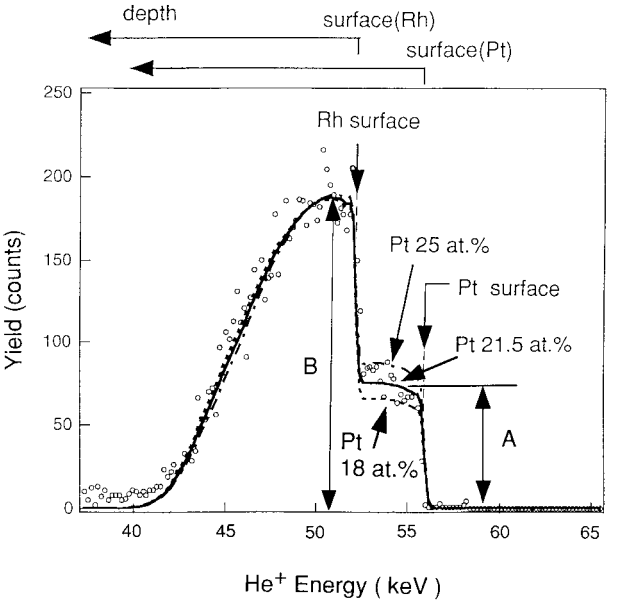

FIG. 3. MEIS spectra from the Pt–Rh/α-Al_2O_3. The open circles denote the observed spectrum. The solid, dashed, and dash-dotted curves denote the simulated spectra assuming the Pt concentration to be 21.5, 18, and 25 at.%, respectively. The surface positions of Pt and Rh are indicated by arrows.

Figure 3 displays the MEIS spectrum of Pt–Rh/α-Al_2O_3. In Fig. 3, the horizontal axis denotes scattered He energy, and it is converted into the depth from the surface of a sample for each element (shown above the spectrum). The vertical axis denotes the yield of scattered He particles. The Pt surface concentration is obtained by the spectrum height at the Pt surface (A). The Rh surface concentration is determined by the spectrum height (B-A) since the spectrum height at about 50 keV is composed of the yield from Rh at the surface and the yield from Pt in a somewhat deeper region. In the figure, circles denote the observed spectrum, and the dashed, solid, and dash-dotted curves are the simulation spectra calculated assuming Pt atomic concentration 18, 21.5, and 25 at%, respectively. In all the simulated curves, the particle radii were assumed to be the same, 1.08×10^{17} cm^{-2} (which corresponds to 15.2 nm in ordinary radius, using an atomic density of 7.12 atom/cm^3 for the 0.2 : 0.8 Pt/Rh particles). Although the measured spectrum shows some scatter, the yield corresponding to Pt falls onto the area between the simulated spectra calculated for Pt 25 at% and Pt 18 at%. The best-fitted spectrum was obtained with Pt 21.5 at%. Thus the composition near the surface can be determined within an error of about ±4%. In deeper regions, however, the composition could not be determined due to the overlap of the peaks of Pt and Rh.

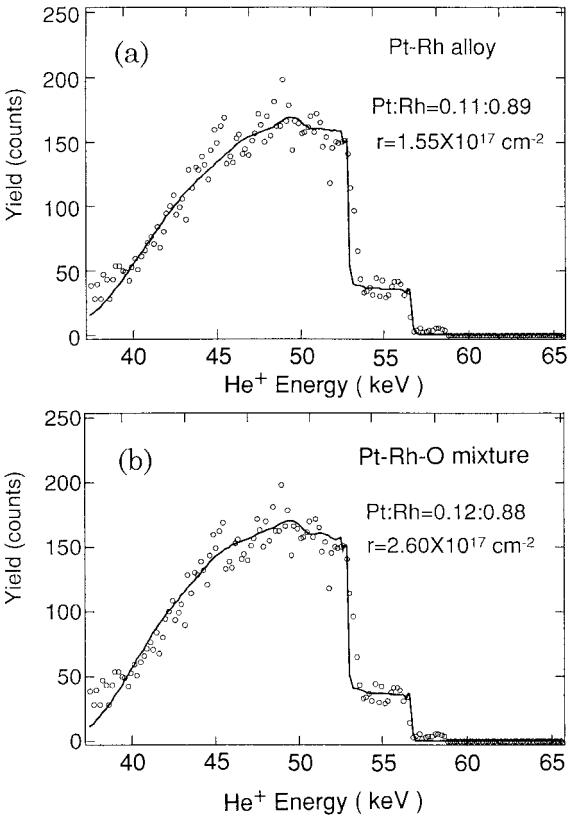

FIG. 4. MEIS spectra from the Pt–Rh/α-Al_2O_3 after heat treatment in oxidative atmosphere (800°C, 3 h in O_2 7.5%, N_2 92.5%). The open circles denote the observed spectrum. The solid curves denote the simulated spectrum obtained assuming Pt–Rh particles to be (a) Pt–Rh alloy and (b) Pt–Rh–O mixture.

Figure 4 displays the spectra of the sample after oxidative treatment (800°C, 3 h in O_2 7.5%, N_2 92.5%). Figure 4a is the spectrum obtained assuming that the metal particles are Pt–Rh alloy. The average particle radius has grown to 1.55×10^{17} cm^{-2}, where the radius before oxidative treatment was 1.08×10^{17} cm^{-2}. The Pt/Rh ratio near the surface was determined to be Pt : Rh = 0.11 : 0.89, which shows the increase of Pt concentration.

Here, it is more realistic that we assume the particle contains oxygen besides Pt and Rh because Rh is oxidized after the heat treatment in the oxidative environment. Although we were not able to estimate the quantity of oxygen due to the shortage of the yield from oxygen, we tried to simulate the spectrum assuming the Rh/O ratio to be 2/3 according to the composition of Rh oxide (Rh_2O_3). The best-fitted spectrum was obtained as shown in Fig. 4b. The Pt/Rh ratio near the surface was Pt : Rh = 0.12 : 0.88, which reproduced the results of Fig. 4a. The average particle radius obtained was 2.60×10^{17} cm^{-2}, which is larger than the result of Fig. 4a because of the existence of oxygen naturally.

Figure 5 displays the spectrum of the sample after reductive treatment (800°C, 1 h in H_2 4%, N_2 96%) of the

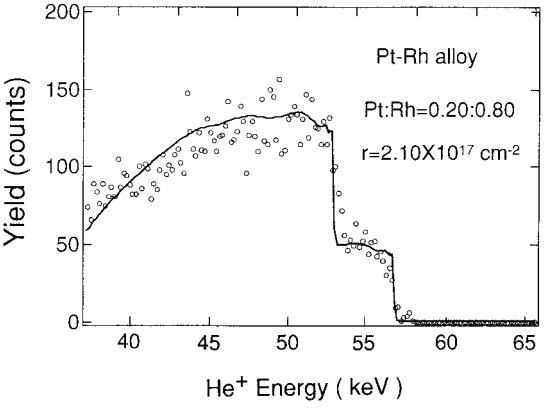

FIG. 5. MEIS spectra from the Pt–Rh/α-Al_2O_3 after heat treatment in reductive atmosphere (800°C, 1 h in H_2 4%, N_2 96%). The open circles denote the observed spectrum. The solid curve denotes the simulated spectrum obtained assuming Pt–Rh particles to be Pt–Rh alloy.

oxidative-treated sample. It shows that the average particle radius increased to 2.10×10^{17} cm^{-2} (29.5 nm in ordinary radius) and that the Pt/Rh ratio near the surface region returned to its original value of Pt : Rh = 0.20 : 0.80.

3.2. Particle Size Evaluation

First, we simulated the spectrum of Pt particles, varying the particle size in order to confirm the applicability of the simulation to the evaluation of average particle size. Figure 6 displays the simulated MEIS spectra of Pt/α-Al_2O_3 for the particle radii 10, 20, 40, and 100×10^{15} cm^{-2}, which are converted into ordinary radii as 1.5, 3.0, 6.0, and 15.1 nm, respectively. As shown in Fig. 6, the width of the spectrum peak increases with increased particle radius. This result indicates that we can evaluate the changes in the average radius of particles in the region below 10 nm using this simulation.

Second, we examined the applicability of the simulation to particle size distribution. We assumed the Pt particle size

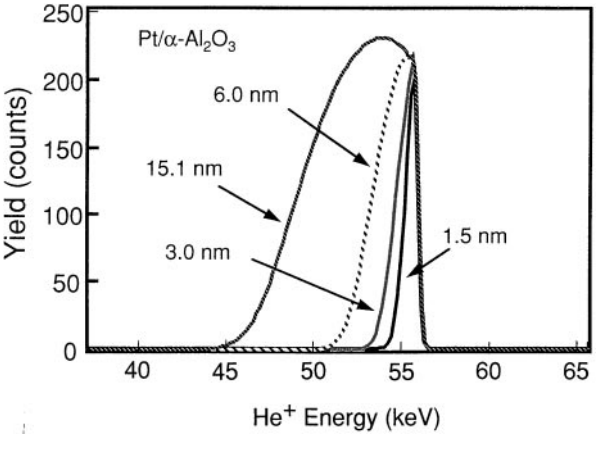

FIG. 6. Simulated MEIS spectra for Pt/α-Al_2O_3. The radii of Pt particles were assumed to be 1.5, 3.0, 6.0, and 15.1 nm.

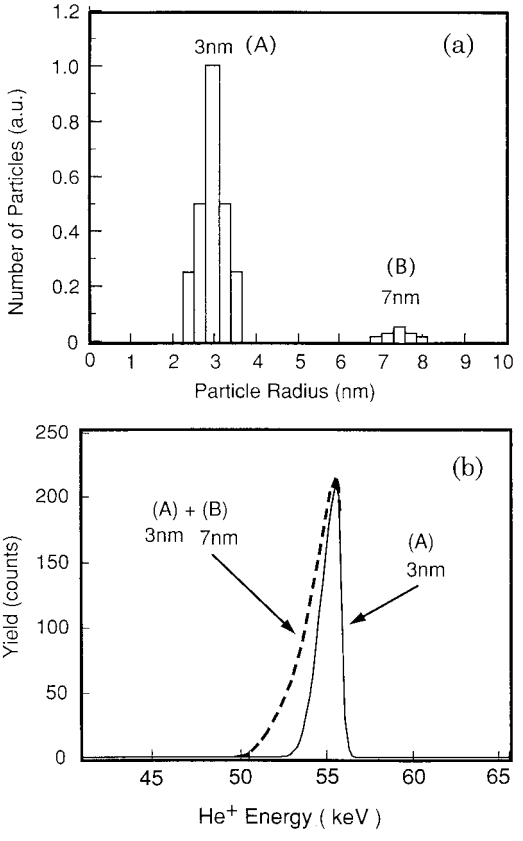

FIG. 7. (a) The Pt particle size distribution for the simulation. (b) Simulated MEIS spectra changing the Pt particle size distribution. The solid and dashed curves denote the spectra obtained with Pt particle size distributions (A) and (A) + (B), respectively.

distribution shown in Fig. 7a. For a particle size distribution like this, XRD would give the average size of the particles as 7–8 nm, while the catalytic activity would indicate that the particles may be much finer, as is often the case with actual catalyst development. When metal particles have the particle size distribution of (A), the corresponding MEIS spectrum is obtained as shown by the solid line in Fig. 7b. If metal particles have the particle size distribution of not only (A) but also (B), the corresponding Pt peak shown with the dotted line in Fig. 7b has some tail. Thus, we can distinguish particle size distribution from the change in the spectrum shape.

4. DISCUSSION

In Section 3.1, in the simulation of the spectrum for Pt–Rh particles after oxidative and reductive treatment we assumed that they consisted of Pt–Rh alloy or Pt–Rh–O mixture. The reason for this assumption is as follows.

From our FE-SEM observations of Pt–Rh/α-Al_2O_3 samples after oxidative treatment, we observed images of the particles which were completely different from images of Pt/α-Al_2O_3 samples after the same treatment. That is, the Pt particles in the Pt/α-Al_2O_3 sample were round and grew remarkably while the particles in the Pt–Rh/α-Al_2O_3 sample did not have a round shape and they grew much less than Pt particles. If Pt sinters more rapidly than Rh and Rh oxide is separated from the original Pt–Rh alloy after oxidation (as in the case of the Pt–Ir system reported in Ref. (16)), two different kinds of particles (large, round Pt particles and relatively small Rh oxide particles) should be observed separately. That kind of particle segregation, however, was not observed. Therefore, we assumed the particle after oxidation to be a Pt–Rh alloy or a Pt–Rh–O mixture (as mentioned in Section 3.1, a Pt–Rh–O mixture is more realistic after oxidation). Also, since the FE-SEM image of the particles in the Pt–Rh/α-Al_2O_3 sample after reduction was similar to the image of the particles before oxidative and reductive treatment, we assumed the particle to be Pt–Rh alloy after treatment. It has been reported for Rh supported on aluminas that Rh oxides diffuse below the surface of aluminas during oxidative treatment (17). But our RBS analysis showed no diffusion of Rh atoms after oxidation. The reason for not observing Rh diffusion into aluminas may be the difference in the support material structure (in Ref. (17) the support was γ-Al_2O_3, while in our study it was α-Al_2O_3).

Here, we must mention the limitations of this analysis based on this simulation.

(1) As mentioned above, we applied the simulation program assuming the Pt–Rh particles to be an alloy. This information was obtained by FE-SEM observation. Therefore, in general, this analysis (MEIS and this simulation) alone cannot be useful unless it is coupled with other techniques which provide information on whether the particles are alloyed or are composed of individual metals. The usefulness of this simulation is that, once this kind of information is obtained, the quantitative (not qualitative) composition analysis can be performed.

(2) Since the spectra of Pt and Rh were separated near the surface region, we were able to estimate the composition of the particle quantitatively by the simulation developed here. In a lower energy region, however, it is difficult to determine the composition because of the overlap of the Pt and Rh peaks.

(3) In the evaluation of the particle size distribution, there exists a limitation on the application of this simulation, concerning the size of particles which are on a support. In general, scattering yield increases with the number of atoms within a particle, and this means that scattering yield increases in proportion to (particle radius)^3. Therefore, larger particles (which belong to distribution (B) in Fig. 7a, for example) tend to make a major contribution to a spectrum shape, making it difficult to discern the distribution of smaller particles. Considering the discussion above, it can be said that for the simulation to be useful

in giving information on particle size distribution, samples should be in the initial sintering stage of metal particles, where the number of particles which are larger than 10 nm is negligible.

Further extension of the application of this simulation analysis is expected as follows. In this work, the alloy particles were assumed to be uniform within the particle. It should be pointed out that if one element segregates to the top surface and forms a very thin layer, a peak from the segregated element should be observed in the spectrum. For example, one of the models proposed to explain the SMSI (Strong Metal–Support Interaction) effect (18–20) is that the surface of Rh is covered with TiO_x atoms after reductive treatment of Rh particles supported on TiO_2 (20, 21). If the thickness of the top surface layers is almost the same in all the particles, the simulation may be expanded to this kind of top surface segregation by dividing the hemisphere into two layers. In this case, the thickness of the layers and their composition would be obtained from the peak width and the peak height, respectively.

5. CONCLUSION

A MEIS spectrum simulation program has been developed for the analysis of metal particles using a Monte Carlo algorithm. The program was applied to the composition and particle size analysis of Pt–Rh/α-Al_2O_3 treated in oxidative and reductive environments. A quantitative composition analysis has been attained, and it has been shown that Pt concentration decreased after oxidative treatment and returned to its original value after reductive treatment. Also, quantitative evaluation of particle sizes less than 10 nm has been made possible by this simulation program. In addition, this simulation gives us some information on particle size distribution in the initial stage of particle sintering, which has been out of the reach of conventional analytical tools. The limitation of the estimation of particle size distribution using this method resides in the existence of larger particles.

ACKNOWLEDGMENTS

The authors thank A. Kawano, K. Yokota, and S. Noda for helpful discussions and encouragement.

REFERENCES

1. Matsunaga, S., Yokota, K., Hyodo, S., Suzuki, T., and Sobukawa, H., SAE Paper 982706, 1998.
2. Fiedorow, R. M. J., and Wanke, S. E., *J. Catal.* **43**, 34 (1976).
3. Fiedorow, R. M. J., Chahar, B. S., and Wanke, S. E., *J. Catal.* **51**, 193 (1978).
4. Yao, H. C., Japar, S., and Shelef, M., *J. Catal.* **50**, 407 (1977).
5. Cullity, B. D., "Elements of X-Ray Diffraction," 2nd ed., Addison–Wesley, Reading, MA, 1978.
6. Okumura, K., Hyodo, S., Noda, S., and Maruyama, Y., *J. Phys. Chem.* **102**, 2350 (1998).
7. Veen, J. F., *Surf. Sci. Rep.* **5**, 199 (1985).
8. Turkenburg, W. C., Soszka, W., Saris, F. W., Kersten, H. H., and Colenbrander, B. G., *Nucl. Instrum. Meth.* **132**, 587 (1976).
9. Ziegler, J. F., "Helium Stopping Powers and Ranges in All Elements," Vol. 4. Pergamon, New York, 1977.
10. Molière, G., *Z. Naturforsch. A* **2**, 133 (1947).
11. Chu, W. K., Mayer, J. W., and Nicolet, M. A., "Backscattering Spectrometry." Academic Press, Orlando, 1978.
12. Chu, W. K., *Rhys. Rev. A* **13**, 2057 (1976).
13. Kido, Y., and Koshikawa, T., *J. Appl. Phys.* **67**, 187 (1990).
14. Marion, J. B., and Young, F. C., "Nuclear Reaction Analysis—Graphs and Tables." North-Holland, Amsterdam, 1968.
15. Konomi, I., Kawano, A., and Kido, Y., *Surf. Sci.* **207**, 427 (1988).
16. Sinfelt, J. H., and Via, G. H., *J. Catal.* **56**, 1 (1979).
17. Wong, C., and McCabe, R. W., *J. Catal.* **119**, 47 (1989).
18. Tauster, S. J., Fung, S. C., and Garten, R. L., *J. Am. Chem. Soc.* **100**, 170 (1978).
19. Tauster, S. J., Fung, S. C., Baker, R. T. K., and Horsley, J. A., *Science* **211**, 1121 (1981).
20. Resasco, D. E., and Haller, G. L., *J. Catal.* **82**, 279 (1983).
21. Sadeghi, H. R., and Henrich, V. E., *J. Catal.* **87**, 279 (1984).